The Astrophysical Journal, 839:95 (9pp), 2017 April 20 https://doi.org/10.3847/1538-4357/aa6a19

Late-time Cooling of Neutron Star Transients and the Physics of the Inner Crust

Alex Deibel[1,2], Andrew Cumming[2,3], Edward F. Brown[1,2,4], and Sanjay Reddy[2,5]
[1] Department of Physics and Astronomy, Michigan State University, East Lansing, MI 48824, USA; deibelal@msu.edu
[2] The Joint Institute for Nuclear Astrophysics—Center for the Evolution of the Elements, Michigan State University, East Lansing, MI 48824, USA
[3] Department of Physics and McGill Space Institute, McGill University, 3600 rue University, Montreal, QC H3A 2T8, Canada
[4] National Superconducting Cyclotron Laboratory, Michigan State University, East Lansing, MI 48824, USA
[5] Institute for Nuclear Theory, University of Washington, Seattle, WA 98195-1550, USA
Received 2016 September 22; revised 2017 March 20; accepted 2017 March 27; published 2017 April 20

Abstract

An accretion outburst onto a neutron star transient heats the neutron star's crust out of thermal equilibrium with the core. After the outburst, the crust thermally relaxes toward equilibrium with the neutron star core, and the surface thermal emission powers the quiescent X-ray light curve. Crust cooling models predict that thermal equilibrium of the crust will be established ≈1000 days into quiescence. Recent observations of the cooling neutron star transient MXB 1659-29, however, suggest that the crust did not reach thermal equilibrium with the core on the predicted timescale and continued to cool after ≈2500 days into quiescence. Because the quiescent light curve reveals successively deeper layers of the crust, the observed late-time cooling of MXB 1659-29 depends on the thermal transport in the inner crust. In particular, the observed late-time cooling is consistent with a low thermal conductivity layer near the depth predicted for nuclear pasta that maintains a temperature gradient between the neutron star's inner crust and core for thousands of days into quiescence. As a result, the temperature near the crust–core boundary remains above the critical temperature for neutron superfluidity, and a layer of normal neutrons forms in the inner crust. We find that the late-time cooling of MXB 1659-29 is consistent with heat release from a normal neutron layer near the crust–core boundary with a long thermal time. We also investigate the effect of inner crust physics on the predicted cooling curves of the accreting transient KS 1731-260 and the magnetar SGR 1627-41.

Key words: dense matter – stars: neutron – X-rays: binaries – X-rays: individual (MXB 1659-29, KS 1731-260, SGR 1627-41)

1. Introduction

An accretion outburst onto a neutron star transient triggers non-equilibrium nuclear reactions (Bisnovatyĭ-Kogan & Chechetkin 1979; Sato 1979) that deposit heat in the neutron star's crust (Haensel & Zdunik 1990, 2003, 2008). Accretion-driven heating brings the crust out of thermal equilibrium with the core; when accretion ceases, the crust cools toward thermal equilibrium with the core and powers the quiescent light curve (Brown et al. 1998; Ushomirsky & Rutledge 2001; Rutledge et al. 2002). Brown & Cumming (2009) discussed the basic idea that observations at successively later times into quiescence probe successively deeper layers in the crust with increasingly longer thermal times. In particular, about a year into quiescence the shape of the cooling light curve is sensitive to the physics of the inner crust at mass densities greater than neutron drip $\rho \gtrsim \rho_{\rm drip} \approx 4 \times 10^{11}\,{\rm g\,cm^{-3}}$ (Page & Reddy 2012).

Among the modeled cooling transients, MXB 1659-29 (Wijnands et al. 2003, 2004; Cackett et al. 2008) was thought to be unique in that its crust appeared to reestablish its long-term thermal equilibrium with the core after ≈1000 days into quiescence (Brown & Cumming 2009). Recent observations of MXB 1659-29 (Cackett et al. 2013), however, indicate that the crust continued to cool after ≈2500 days to reach a new low temperature when observed ≈4000 days into quiescence. Although the drop in count rate could be explained by a change in absorption column, for example, due to a build up of an accretion disk in the binary, it is also consistent with a drop in neutron star effective temperature.

Horowitz et al. (2015) show that the late-time drop in temperature in MXB 1659-29 could be caused by a low thermal conductivity layer at the base of the inner crust at a mass density $\rho \gtrsim 8 \times 10^{13}\,{\rm g\,cm^{-3}}$. The low thermal conductivity may be a consequence of nuclear pasta, which forms when nuclei are distorted into various complex shapes at high densities in the inner crust (Ravenhall et al. 1983; Hashimoto et al. 1984; Oyamatsu 1993). Nuclear pasta has been studied using quantum molecular dynamics simulations (Maruyama et al. 1998; Watanabe et al. 2003) and semi-classical molecular dynamics simulations (Horowitz et al. 2004; Horowitz & Berry 2008; Schneider et al. 2013), but the thermal properties of nuclear pasta remain uncertain. Horowitz et al. (2015) discovered a possible mechanism for lowering the electrical and thermal conductivity of pasta, finding spiral defects in molecular dynamics simulations of pasta that could act to scatter electrons. They demonstrate that a signature of the low conductivity pasta layer would be in the thermal behavior of the crust and they show that models of crust cooling in MXB 1659-29 that include a low conductivity pasta layer can account for the observed drop in count rate. Similarly, a low electrical conductivity layer has been suggested by Pons et al. (2013) to explain the puzzling cutoff in the spin period distribution of pulsars at $P \sim 10$ s, and they suggest the low electrical conductivity layer may be associated with a nuclear pasta phase deep in the crust.

The quasi-free neutrons that coexist with nuclear pasta in the deep inner crust also impact late-time crust cooling (Page & Reddy 2012). The critical temperature T_c of the $^1S_0$ neutron singlet pairing gap is expected to increase from zero near

neutron drip to a maximum value near $T_c \gtrsim 10^9$ K before decreasing again at high mass densities where the repulsive core of the neutron interaction removes the tendency to form pairs. Calculation of the critical temperature, however, is complicated by the influence of the nuclear clusters, and a wide range of predictions for $T_c(\rho)$ have been made in the literature (e.g., see the plot in Page & Reddy 2012 and references therein). One of the uncertain aspects of the pairing gap is whether the $^1S_0$ gap closes before or after the crust–core transition (Chen et al. 1993). If the gap closes before the crust–core transition and there is a low thermal conductivity pasta layer, a layer of normal neutrons will persist near the base of the crust where $T > T_c$, significantly increasing its heat capacity. Here, we show that a normal neutron layer with a large heat capacity leaves a signature in the cooling curve at late times and a crust cooling model with normal neutrons gives the best fit to the quiescent cooling observed in MXB 1659-29.

The months to years long flux decays following magnetar outbursts have also been successfully fit with crust thermal relaxation models (e.g., Lyubarsky et al. 2002; Pons & Rea 2012; Scholz et al. 2014). Many uncertainties remain, including the origin of the X-ray spectrum, the nature of the heating event that drives the outburst, and the role of other heat sources such as magnetospheric currents (Beloborodov 2009). Despite this, magnetar flux decays are interesting because the decay can span a large range of luminosity, and because multiple outbursts from the same source can be studied. The outburst models typically require energy injection into the outer crust of the star, but a significant amount of energy is conducted inward to the core. Late-time observations as the magnetar's crust relaxes may then probe the thermal properties of the inner crust.

We investigate the role of a low thermal conductivity pasta layer and normal neutrons in cooling neutron stars in more detail in this paper. In Section 2, we outline our model of the crust cooling in MXB 1659-29, highlighting the important role of the density dependence of the neutron superfluid critical temperature near the crust–core transition. In Section 3, we discuss late-time cooling in other sources, including the accreting neutron star KS 1731-260 and the magnetar SGR 1627-41. We conclude in Section 4.

2. The Late Time Cooling of MXB 1659-29

2.1. Crust Cooling Model and the Role of the Normal Neutron Layer at the Base of the Crust

We follow the thermal evolution of the neutron star crust using the thermal evolution code `dStar` (Brown 2015) that solves the fully general relativistic heat diffusion equation using a method of lines algorithm in the `MESA` numerical library (Paxton et al. 2011, 2013, 2015). The microphysics of the crust follows Brown & Cumming (2009). The results are verified with the code `crustcool`[6] that solves the heat diffusion equation assuming constant gravity through the crust.

We model the ≈2.5 year outburst in MXB 1659-29 (Wijnands et al. 2003, 2004) using a local mass accretion rate $\dot{m} = 0.1\,\dot{m}_{\rm Edd}$, where $\dot{m}_{\rm Edd} = 8.8 \times 10^4$ g cm^{-2} s^{-1} is the local Eddington mass accretion rate. The model uses a neutron star mass of $M = 1.6\,M_\odot$ and radius of $R = 11.2$ km that are consistent with the MXB 1659-29 quiescent light curve fits from Brown & Cumming (2009). The model includes a $Q_s = 1$ MeV per accreted nucleon shallow heat source spread between $y = 2 \times 10^{13}$ g cm^{-2} and $y = 2 \times 10^{14}$ g cm^{-2}, in addition to deep crustal heating from electron capture and pycnonuclear reactions (Haensel & Zdunik 1990, 2003, 2008). For the crust composition we use the accreted composition from Haensel & Zdunik (2008) that assumes an initial composition of pure ^{56}Fe (see their Table A3).

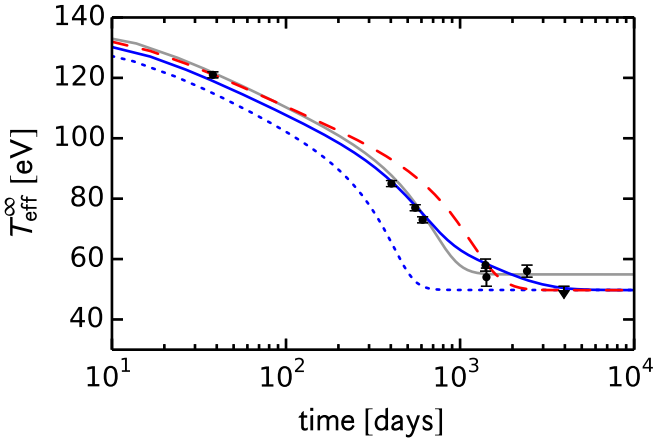

Figure 1. Cooling models for MXB 1659-29. The solid gray curve is a model that uses $Q_{\rm imp} = 2.5$ throughout the entire crust and $T_{\rm core} = 4 \times 10^7$ K. The solid blue curve is a model with $Q_{\rm imp} = 20$ for $\rho > 8 \times 10^{13}$ g cm^{-3}, $Q_{\rm imp} = 1$ for $\rho < 8 \times 10^{13}$ g cm^{-3}, $T_{\rm core} = 3.25 \times 10^7$ K, and using the G08 pairing gap. The dashed red curve uses the same $Q_{\rm imp}$ as the solid blue curve, but with the S03 pairing gap. The dotted blue curve is a model with the G08 pairing gap and $Q_{\rm imp} = 1$ throughout the crust, but without a low thermal conductivity pasta layer.

The thermal conductivity in the inner crust is largely set by impurity scattering. The impurity parameter of the crust is given by

$$Q_{\rm imp} \equiv \frac{1}{n_{\rm ion}} \sum_j n_j (Z_j - \langle Z \rangle)^2, \quad (1)$$

where $n_{\rm ion}$ is the number density of ions, n_j is the number density of the nuclear species with Z_j number of protons, and $\langle Z \rangle$ is the average proton number of the crust composition. The impurity parameter in the neutron star crust was constrained to $Q_{\rm imp} < 10$ in MXB 1659-29 (Brown & Cumming 2009) assuming a constant impurity parameter throughout the entire crust. We show a model of crust cooling in MXB 1659-29 with $Q_{\rm imp} = 2.5$ and $T_{\rm core} = 4 \times 10^7$ K, consistent with the fit from Brown & Cumming (2009), in Figure 1. In this model, the crust reaches thermal equilibrium with the core by ≈1000 days into quiescence, and so predicts a constant temperature at later times.

We also run two models with a disordered inner crust with $Q_{\rm imp} = 20$ for $\rho > 8 \times 10^{13}$ g cm^{-3} (and $Q_{\rm imp} = 1$ for $\rho < 8 \times 10^{13}$ g cm^{-3}) to represent the low conductivity expected for nuclear pasta, as done in Horowitz et al. (2015); both models have a neutron star mass $M = 1.6\,M_\odot$, radius $R = 11.2$ km, and $T_{\rm core} = 3 \times 10^7$ K. The two models use different choices of the neutron superfluid critical temperature profile $T_c(\rho)$. The first uses a $^1S_0$ gap that closes in the inner crust (Gandolfi et al. 2008, hereafter G08), and the second uses a gap that closes in the core (Schwenk et al. 2003, hereafter

[6] https://github.com/andrewcumming/crustcool

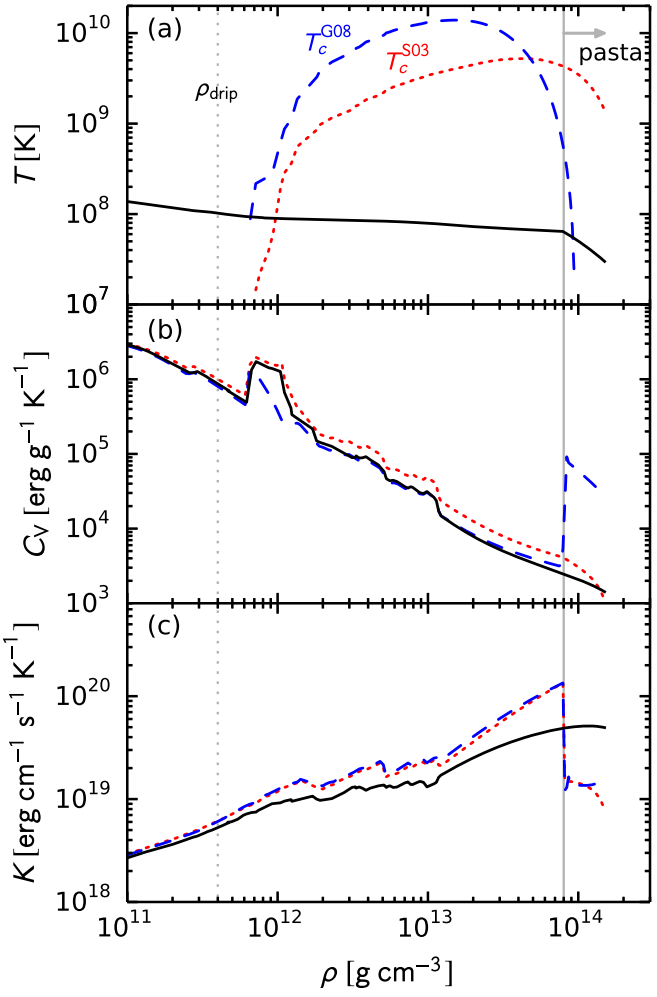

Figure 2. Thermal transport in the inner crust of MXB 1659-29 at the start of quiescence. The gray vertical lines indicate the neutron drip density and the transition to nuclear pasta. Panel (a): the temperature profile (solid curve) corresponding to the cooling model in Figure 1 with a $Q_{\rm imp} = 20$ pasta layer and the G08 pairing gap. The dashed curves show two choices for $T_c(\rho)$; the blue dashed curve corresponds to G08 and the red dotted curve is S03. Panel (b): the heat capacity profiles for the same models as Figure 1. Solid black curve: $Q_{\rm imp} = 3.7$ throughout the inner crust. Dashed blue curve: $Q_{\rm imp} = 20$ for $\rho > 8 \times 10^{13}$ g cm^{-3} and $Q_{\rm imp} = 1$ for $\rho < 8 \times 10^{13}$ g cm^{-3} using the G08 pairing gap that closes in the crust. Dotted red curve: same as the dashed curve, but with a different choice for $T_c(\rho)$ from the S03 pairing gap that closes in the core. Panel (c): thermal conductivity profiles for the same models.

S03). The difference in the $T_c(\rho)$ profiles for each pairing gap model are shown in Figure 2.

As can be seen in Figure 1, the solid blue curve corresponding to the G08 gap shows a long decline in temperature even at late times near ≈4000 days, and thermal equilibrium is reached near ≈5000 days into quiescence. Note, however, that is difficult to reproduce the observations near ≈1500 days and ≈2500 days simultaneously. By contrast, the red dashed curve using the S03 gap does not show a decline at late times, but instead levels off to a constant temperature after ≈2000 days. This difference arises because significant late-time cooling only occurs if there is a normal layer of neutrons at the base of the crust, giving a large heat capacity there (Figure 2). Furthermore, as demonstrated by the blue dotted curve in Figure 1, crust cooling with normal neutrons, but without a low thermal conductivity pasta layer, does not exhibit late-time cooling.

As we show in the following section, a low conductivity pasta layer maintains a temperature difference between the inner crust and core during quiescence, and a layer of normal neutrons survives at the base of the crust that has a long thermal time.

2.2. Analytic Estimates

Some analytic estimates are useful to understand why the late-time cooling occurs and the crucial role of the normal neutron layer. First, we consider the temperature contrast ΔT between the inner crust and the core that develops during the accretion outburst. This is set by the value at which the heat flux through the pasta layer balances the nuclear heating in the crust (mostly located at shallower densities near the neutron drip region). The heating rate is $\epsilon_{\rm nuc} = \dot{m} E_{\rm nuc}$, where $E_{\rm nuc} \approx 2$ MeV per accreted nucleon comes from deep crustal heating. The equivalent heat flux is $F_{\rm in} \approx 2 \times 10^{22}$ erg cm^{-2} s^{-1} for an accretion rate of $\dot{m} = 0.1\, \dot{m}_{\rm Edd}$.

The heat flux through the pasta layer is $F \approx K \Delta T / H$, where K is the thermal conductivity and H the pressure scale height. Neutrons set the pressure in the inner crust, so that[7] $H = P/\rho g \approx 7 \times 10^4$ cm $(\rho_{14}^{2/3} Y_n^{5/3}/g_{14})$, where Y_n is the neutron fraction, ρ_{14} is the mass density in units of 10^{14} g cm^{-3}, and the surface gravity of the neutron star is $g = (GM/R^2)(1 - 2GM/Rc^2)^{-1/2}$ in units of 10^{14} cm s^{-2}. The thermal conductivity is primarily set by electron–impurity scattering, with scattering frequency (Itoh & Kohyama 1993; Potekhin et al. 1999)

$$\nu_{eQ} = \frac{4\pi e^4 n_e}{p_{{\rm F},e}^2 v_{{\rm F},e}} \frac{Q_{\rm imp}}{\langle Z \rangle} \Lambda_{eQ} \tag{2}$$

$$\approx 3 \times 10^{18}\ {\rm s}^{-1} \left[\left(\frac{\rho_{14} Y_e}{0.05} \right)^{1/3} \left(\frac{Q_{\rm imp} \Lambda_{eQ}}{\langle Z \rangle} \right) \right]. \tag{3}$$

Here, $p_{{\rm F},e}$ and $v_{{\rm F},e}$ and the Fermi momentum and velocity of the electrons, Λ_{eQ} is the Coulomb logarithm, and Y_e is the electron fraction. The quantity $Q_{\rm imp}\Lambda_{eQ}/\langle Z \rangle$ is of order unity in the inner crust. The resulting thermal conductivity is

$$K_e = \frac{\pi}{12} \frac{E_{{\rm F},e}\, k_{\rm B}^2\, Tc}{e^4} \frac{\langle Z \rangle}{Q_{\rm imp} \Lambda_{eQ}}$$

$$\approx 4 \times 10^{19}\ {\rm erg\ s^{-1}\ cm^{-1}\ K^{-1}} \left[T_8 \left(\frac{\rho_{14} Y_e}{0.05} \right)^{1/3} \frac{\langle Z \rangle}{Q_{\rm imp} \Lambda_{eQ}} \right], \tag{4}$$

where $T_8 \equiv T/(10^8\ {\rm K})$. Therefore, the temperature difference between inner crust and core is

$$\Delta T \approx 3 \times 10^7\ {\rm K} \times \left[\frac{\rho_{14}^{1/3}}{g_{14} T_8} \frac{Y_n^{5/3}}{(Y_e/0.05)^{1/3}} \left(\frac{Q_{\rm imp} \Lambda_{eQ}}{\langle Z \rangle} \right) \left(\frac{\dot{m}}{0.1 \dot{m}_{\rm Edd}} \right) \right], \tag{5}$$

which is in reasonable agreement with the temperature jumps seen in Figure 2(a) between $\rho \approx 8 \times 10^{13}$ g cm^{-3} and $\rho \approx 1.5 \times 10^{14}$ g cm^{-3}.

[7] In the inner crust, $\Gamma_1 \equiv (\partial \ln P/\partial \ln \rho)_s$ varies with density: at first, Γ_1 decreases below 4/3 (the value for degenerate relativistic electrons) and then it increases for $\rho \gtrsim 10^{13}$ g cm^{-3} and approaches $\Gamma_1 \lesssim 2$ at roughly nuclear density. For definiteness in computing H, we set $\Gamma_1 = 5/3$.

We can understand the cooling timescale of the normal neutron layer as follows. The specific heat capacity of the normal neutrons is

$$C_V = \frac{\pi^2}{\rho}\frac{n_n k_B^2 T}{p_{F,n} v_{F,n}} \approx 3 \times 10^4 \text{ erg g}^{-1} \text{ K}^{-1} \left[Y_n^{1/3} \rho_{14}^{-2/3} \left(\frac{T_7}{3} \right) \right], \quad (6)$$

where n_n is the number density of free neutrons, $p_{F,n}$ is the neutron Fermi momentum, and $v_{F,n}$ is the neutron Fermi velocity. The thermal diffusivity is

$$D = \frac{K}{\rho C_V} \approx 4 \text{ cm}^2 \text{ s}^{-1} \left(\frac{Y_e}{0.05 Y_n} \right)^{1/3} \left(\frac{\langle Z \rangle}{Q_{\rm imp} \Lambda_{eQ}} \right); \quad (7)$$

D is independent of temperature and depends only weakly on density. The thermal timescale is then

$$t_{\rm therm} \approx \frac{H^2}{D} \approx 4000 \text{ days} \left[\rho_{14}^{4/3} Y_n^{11/3} \left(\frac{g_{14}}{2} \right)^{-2} \left(\frac{Q_{\rm imp} \Lambda_{eQ}}{\langle Z \rangle} \right) \left(\frac{Y_e}{0.05} \right)^{-1/3} \right] \quad (8)$$

Again, this is in good agreement with the cooling timescale we see in the numerical models. It also highlights the role of the large heat capacity from the normal neutrons. Without the normal neutrons, the electrons would set the heat capacity in the inner crust (see, e.g., Figure 6 of Brown & Cumming 2009); in this case, the thermal conductivity is $K = \rho C_V^e v_{F,e}^2 / 3\nu_{eQ}$, where C_V^e is the heat capacity of electrons, and we see that the thermal diffusivity is then $D \approx c^2/3\nu_{eQ}$, which is about two orders of magnitude larger than that given by Equation (7). Without normal neutrons, the inner crust cools in months, so that no late-time cooling signature of the pasta region is seen.

2.3. Effect of Thermal Conduction by Neutrons

The large heat capacity of the normal neutrons suggests they may have a large thermal conductivity that could contribute significantly to the thermal conductivity near the base of the crust. Heat conduction by normal neutrons has been considered in the neutron star core (e.g., Baiko et al. 2001), but not in the crust. We calculate the scattering frequency for neutrons scattering from nuclei in the inner crust, either from thermal vibrations (phonons) or irregularities in the structure (impurities). The details are given in the Appendix; the total scattering frequency is given in Equation (24). The neutron

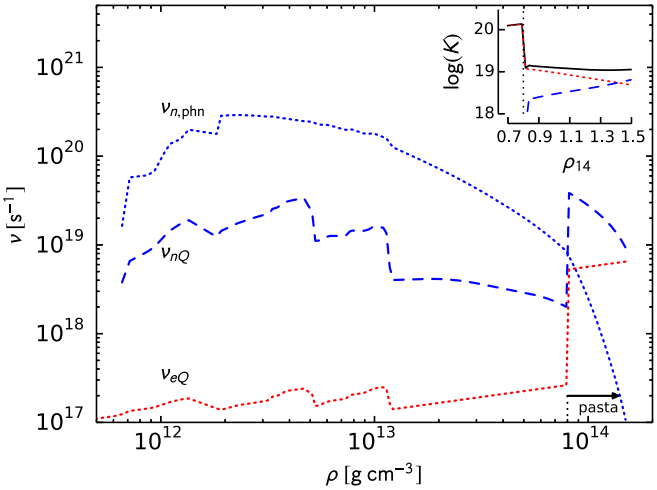

Figure 3. Scattering frequencies in the inner crust at the beginning of quiescence for the model with $Q_{\rm imp} = 20$ at $\rho > 8 \times 10^{13}$ g cm^{-3}, $Q_{\rm imp} = 1$ at $\rho < 8 \times 10^{13}$ g cm^{-3}, and the pairing gap that closes in the crust (Gandolfi et al. 2008). Inset: thermal conductivity K from electron scattering (dotted red curve), neutron scattering (dashed blue curve), and from both electrons and neutrons (solid black curve). The mass density ρ is given in units of 10^{14} g cm^{-3}. The region containing nuclear pasta is to the right of the vertical black dotted line.

thermal conductivity is then $K = \pi^2 n_n k_B^2 T/(3 m_n^\star \nu)$, or

$$K_n = \frac{9\pi^3}{4}\frac{n_n k_B^2 T}{m_n^\star}\frac{\hbar}{m_n^\star c^2}\frac{n_n}{n_{\rm ion}}\left(\frac{\hbar c}{V_0 R_A}\right)^2 \left[\Lambda_{n,\rm phn} + \frac{Q_{\rm imp}}{\langle Z \rangle^2}\Lambda_{nQ}\right]^{-1} \approx 3 \times 10^{17} \text{ erg s}^{-1} \text{ cm}^{-1} \text{ K}^{-1} \, T_8 Y_n \rho_{14} \left(\frac{m_n^\star}{m_n}\right)^{-2} \times \left(\frac{n_n/n_{\rm ion}}{100}\right)\left(\frac{\hbar c}{V_0 R_A}\right)^2 \left[\Lambda_{n,\rm phn} + \frac{Q_{\rm imp}}{\langle Z \rangle^2}\Lambda_{nQ}\right]^{-1}. \quad (9)$$

In this expression, $m_n^\star = p_{F,n} \left[\partial \varepsilon(p)/\partial p\right]^{-1}_{p=p_{F,n}}$ is the Landau effective mass and $\varepsilon(p)$ is the neutron single particle energy including the rest mass (see, e.g., Baym & Chin 1976). The dimensionless quantity $V_0 R_A/\hbar c$ is of order unity and measures the strength of the neutron–nucleus interaction; R_A is the typical size of the scattering structure and energy V_0 is the magnitude of the scattering potential. Note that the neutron scattering frequency can be approximately reproduced by making the substitutions $e^2 \rightarrow V_0 R_A$ and $p_{F,e}^2 v_{F,e} \rightarrow p_{F,n}^2 v_{F,n}$ in Equation (2) for the electron–impurity scattering rate. The quantities $\Lambda_{n,\rm phn}$ and Λ_{nQ} are the Coulomb logarithms for phonon and impurity scattering, respectively. As we discuss in the Appendix, we are able to write the impurity scattering for neutrons in terms of the impurity parameter for electron–impurity scattering $Q_{\rm imp}$.

The thermal conductivity of electrons and neutrons is compared in Figure 3 for the crust temperature profile in Figure 2 where we show the separate contributions from phonon and impurity scattering as a function of density. As has been discussed previously, impurity scattering dominates phonon scattering for electrons in the inner crust when $Q_{\rm imp} \gtrsim 1$ (e.g., Brown & Cumming 2009). We find for neutron scattering that the phonon contribution is larger where $Q_{\rm imp} = 1$, and the impurity contribution is larger in the pasta

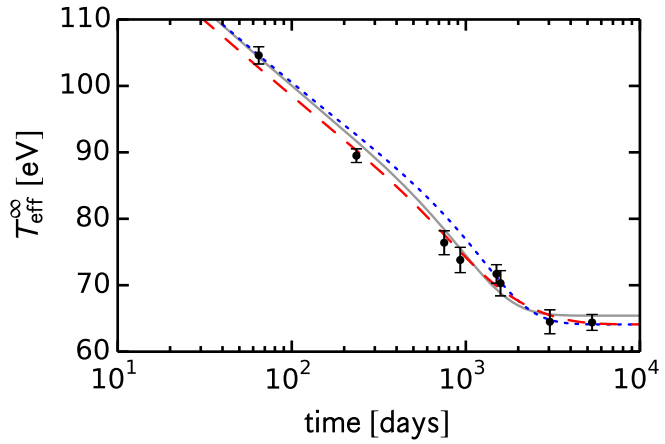

Figure 4. Cooling models for KS 1731-260. Solid gray curve: light curve fit from Merritt et al. (2016) with: $T_c(\rho)$ from Schwenk et al. (2003), a crust impurity parameter of $Q_{\rm imp} = 4.4$, $T_{\rm core} = 9.35 \times 10^7$ K, and no low conductivity pasta layer. Blue dotted curve: a crust impurity parameter of $Q_{\rm imp} = 2$, a pasta impurity of $Q_{\rm imp} = 20$, with $T_c(\rho)$ from Schwenk et al. (2003) and $T_{\rm core} = 9.1 \times 10^7$ K. Red dashed curve: a crust impurity parameter of $Q_{\rm imp} = 2$, a pasta impurity of $Q_{\rm imp} = 20$, with $T_c(\rho)$ from Gandolfi et al. (2008) and $T_{\rm core} = 9.1 \times 10^7$ K.

layer where $Q_{\rm imp} = 20$, as can be seen in Figure 3 (see also Equation (25)).

Figure 3 shows that the conductivity due to neutrons can be comparable to the electron conductivity near the base of the crust, but is otherwise not important. To see this in more detail, it is useful to calculate the ratio K_n/K_e. The electron thermal conductivity is given by Equation (4) and taking the impurity contribution to the neutron conductivity only (since $\nu_{n,\rm phn} \lesssim \nu_{nQ}$ at the base of the crust), we find

$$\frac{K_n}{K_e} = 9\alpha^2 \langle Z \rangle^{2/3} \left(\frac{\hbar c}{V_0 R_A}\right)^2 \frac{\Lambda_{eQ}}{\Lambda_{nQ}} \left(\frac{n_n}{n_{\rm ion}}\right)^{4/3} \left(\frac{v_{{\rm F},n}}{c}\right)^2, \qquad (10)$$

where $v_{{\rm F},n} = p_{{\rm F},n}/m_n^\star$ is the Fermi velocity of the neutrons and $\alpha = e^2/\hbar c \approx 1/137$ is the fine structure constant. All the factors in Equation (10) are <1, except for $n_n/n_{\rm ion}$, which is typically $\sim$100. Therefore, we expect $K_n \lesssim K_e$, consistent with our numerical evaluation shown in Figure 3. Also, since $v_{{\rm F},n} = p_{{\rm F},n}/m_n^\star$, we see that K_n/K_e increases with density approximately as $\rho^{2/3}$, so that neutron thermal conductivity is most important at higher densities. Therefore, we do not expect that neutron thermal conductivity will remove the late-time cooling effect of a disordered pasta layer.

We note that the calculation of the neutron scattering rate could be improved, especially at low temperature and small impurity concentrations. Under these conditions, we found that the scattering rate was large because the neutron–phonon Umklapp process played an important role. In this context, it is known that band gaps in the neutron spectrum can suppress these processes and their effects need to be accounted for before firm conclusions can be drawn, and our estimate should be considered as an upper bound. This uncertainty is unlikely to change our main conclusions, however, since even a modest impurity concentration is sufficient to ensure $K_n < K_e$, except perhaps in the densest layers. In the highest-density regions where pasta phases are likely, the neutron density contrast and therefore V_0 is reduced, which makes neutron scattering less efficient. Here, the details of the neutron density distribution and the appearance of non-spherical rod- and slab-like structures in the pasta region can be important and warrants further study.

An additional piece of physics that could affect late-time cooling is neutrino emission from the pasta layer (Leinson 1993; Gusakov et al. 2004; Newton et al. 2013). To compete with the inward flux of $F_{\rm in} \approx 2 \times 10^{22}$ erg cm^{-2} s^{-1} (see Section 2.2), the neutrino emissivity would have to be $\epsilon_\nu \approx \rho F_{\rm in}/y \sim 10^{18}$ erg cm^{-3} s^{-1} at $T \sim$ (3–6) $\times 10^7$ K. Neutrino cooling in the pasta layer can be enhanced when the neutrons are in the normal phase. Two mechanisms for such enhancement have been considered earlier. In one scenario, enhanced neutrino pair emission arises from spin flip transitions of neutrons due to their spin–orbit interactions with the density gradients in the pasta phase (Leinson 1993). In this case, estimates indicate that the neutrino emissivity $\epsilon_{\nu\bar\nu}^{\rm pasta} \approx 4 \times 10^{23} T_9^6$ erg cm^{-3} s^{-1}. In the second scenario, the direct Urca processes $e^- + p \rightarrow n + \nu_e$ and $n \rightarrow e^- + p + \bar\nu_e$ are kinematically allowed due to coherent Bragg scattering of nucleons from the the pasta (Gusakov et al. 2004); the resulting neutrino emissivity is $\epsilon_{\rm Urca}^{\rm pasta} \approx 4 \times Y_e^{1/3} \times 10^{21} T_9^6$ erg cm^{-3} s^{-1}.

Neutrino emission from electron bremsstrahlung reactions can be enhanced due to impurities since the rate of this reaction is roughly proportional to the electron scattering rate. In earlier work (Ofengeim et al. 2014) it has been shown that in the absence of impurities, when electron–phonon processes dominate, the neutrino energy loss rate at $T = 10^8$ K is about $\epsilon_\nu \sim 10^{13}$ erg cm^{-3} s^{-1} in the pasta region and roughly scales as T^6. This is significantly smaller than the emission expected from normal neutrons, and even a very large enhancement due to impurity scattering is unlikely to be relevant. From these estimates and the preceding discussion we conclude that neutrino cooling in the pasta layers, even with normal neutrons, is unlikely to be relevant at the temperatures encountered during thermal relaxation of the neutron stars and magnetars studied here.

3. Late-time Cooling in Other Sources

3.1. Quasi-persistent Transients

The accreting neutron star KS 1731-260 also has quiescent cooling measurements at late times. Merritt et al. (2016) recently reported a new temperature measurement for KS 1731-260 taken $\approx$5300 days into quiescence. They found that the temperature was consistent with the previous value measured $\approx$3000 days into quiescence, implying that the neutron star crust has now reached thermal equilibrium with the neutron star core near $T_{\rm core} \approx 9.3 \times 10^7$ K. Furthermore, the cooling curve could be fit equally well with or without a disordered pasta layer at the base of the crust. This is a similar result to that found by Horowitz et al. (2015), finding that they could fit KS 1731-260 equally well with or without a disordered pasta layer. The role of the normal neutrons, however, has not been examined in the late-time cooling in this source.

We now model the quiescent cooling of KS 1731-260 following its $\approx$12.5 year outburst including a disordered pasta layer and the G08 gap that closes in the crust. The model uses a neutron star mass $M = 1.4\,M_\odot$ and radius $R = 10$ km, consistent with the spectral fits and crust models from Merritt et al. (2016). The model uses an iron envelope and an accretion rate $\dot m = 0.1\,\dot m_{\rm Edd}$ as done in Merritt et al. (2016) and

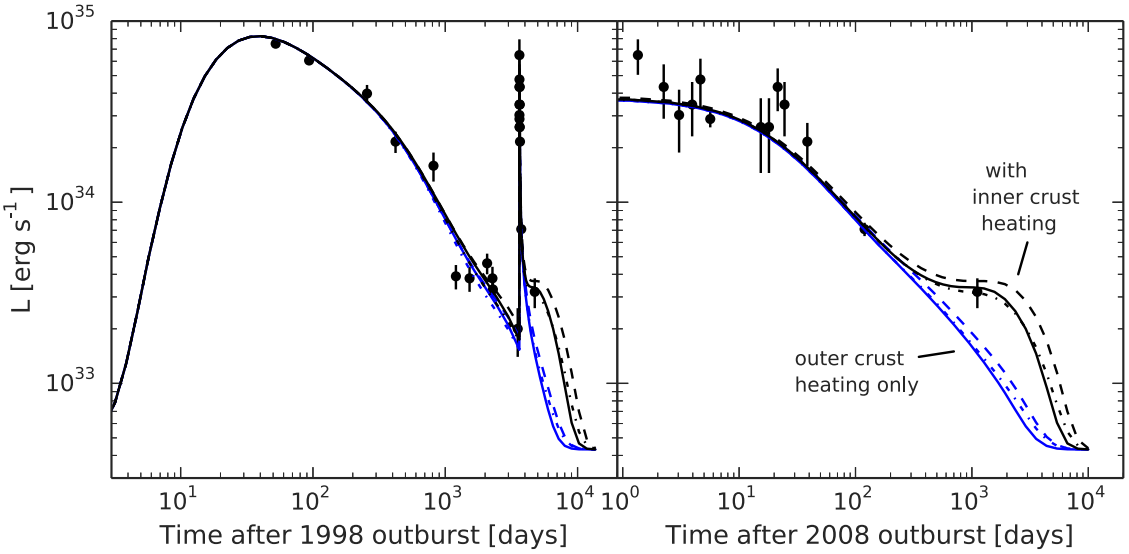

Figure 5. Cooling models for the 1998 and 2008 outbursts of SGR 1627-41. The left panel shows the full light curve of both outbursts; the right panel shows the light curve as a function of time since the beginning of the second outburst. The black and blue solid curves show models with and without heating in the inner crust. Models in which heating is restricted to the outer crust only cool too quickly to match the observed luminosity 1000 days after the 2008 outburst. In each case, the dashed curve shows the effect of including a disordered pasta layer with $Q_{\rm imp} = 25$ for $\rho > 8 \times 10^{13}$ g cm^{-3}. The dotted–dashed curve shows the effect of choosing a different superfluid critical temperature (case B1 from Page & Reddy 2012 instead of Schwenk et al. 2003 as used for the other models).

Cumming et al. (2017). The model fits to the quiescent cooling of KS 1731-260 can be seen in Figure 4.

Although the cooling of KS 1731-260 can be fit well without a low conductivity pasta layer (Merritt et al. 2016), the cooling model with a $Q_{\rm imp} = 20$ pasta layer and the G08 gap provides a better fit to the data. The fit requires a lower core temperature near $T_{\rm core} \approx 9.1 \times 10^7$ K. The high core temperature means that there is not a large temperature difference ΔT (see Equation (5)) between the inner crust and the core during quiescence. The normal neutrons, however, still release heat at late times and the crust reaches thermal equilibrium with the core near ≈5000 days into quiescence.

3.2. The Magnetar SGR 1627-41

The magnetar SGR 1627-41 has had two outbursts, one in 1998 (Woods et al. 1999) and one in 2008 (An et al. 2012). The measured luminosities are shown in Figure 5. The flux decay following the 1998 outburst was fit with a crust cooling model by Kouveliotou et al. (2003). The energy source for magnetar outbursts is thought to be the decaying magnetic field of the star, but the mechanism driving the outbursts and the distribution of the dissipated energy is not understood at present. Therefore the approach of these cooling models is to attempt to reproduce the observed flux decay by varying the amount of energy deposited and its location within the crust. An et al. (2012) showed that the flux decay after both the 1998 and 2008 outbursts could be reproduced by depositing energy in the outer crust, although with about an order of magnitude difference in the depth and magnitude of the energy deposited ($\sim 10^{44}$ erg at $\rho \lesssim 2 \times 10^{11}$ g cm^{-3} for 1998; $\sim 10^{43}$ erg at $\rho \lesssim 3 \times 10^{10}$ g cm^{-3} for 2008).

The late-time observations of SGR 1627-41 after its 1998 outburst are reminiscent of the drop in flux seen in MXB 1659-29. The luminosity appeared to have leveled off after ≈1000 days, but then showed a drop by a factor of two in an observation at ≈3500 days. Moreover, An et al. (2012) showed that the flux ≈1000 days after the 2008 outburst was similar to the flux at the same time after the 1998 outburst. This is unexpected because the energy deposition in the 2008 outburst is much shallower, and by ≈1000 days the crust should have relaxed to the core temperature and the luminosity should be at its minimum value. An et al. (2012) suggested that perhaps the last flux measurement after the 1998 outburst was a statistical deviation (it is within 2σ of the previous flux value), and that the luminosity seen at ≈1000 days in both outbursts reflects the core temperature. This would mean SGR 1627-41 then has a hot core with a temperature near $T_{\rm core} \approx 10^8$ K.

Here, we pursue the possibility of a colder core (as originally envisioned by Kouveliotou et al. 2003) and investigate whether the drop at ≈3000 days is due to inner crust physics. We model the flux decay of SGR 1627-41 using `crustcool`, which includes envelope models and thermal conductivities that take into account the strong magnetic field (averaged over angle around the star; Scholz et al. 2014). The blue solid curves in Figure 5 show the best-fitting model with a constant energy density deposited in the outer crust. The amount of energy deposited is similar to An et al. (2012). In units of 10^{25} erg cm^{-3}, the 1998 outburst model has an energy density $E_{25} = 13$ deposited in the density range 7×10^9 g cm$^{-3} < \rho < 3 \times 10^{11}$ g cm^{-3}, and the 2008 outburst model has $E_{25} = 1.0$ in the density range 10^9 g cm$^{-3} < \rho < 3 \times 10^{11}$ g cm^{-3}. We set the impurity parameter $Q_{\rm imp} = 3$, constant throughout the crust, and core temperature $T_{\rm core} = 7 \times 10^7$ K (as measured at the crust–core boundary) so that the flux in the 1998 outburst continues to decline at ≈3000 days. As An et al. (2012) pointed out, the 2008 outburst then cools much too quickly to agree with the flux measured at ≈1000 days.

We introduce a pasta layer with $Q_{\rm imp} = 25$ at $\rho > 8 \times 10^{13}$ g cm^{-3} to try to increase the luminosity at ≈1000 days after the 2008 outburst. The light curve is shown as the blue dashed line in Figure 5. Unlike accreting neutron stars, we find that introducing a low conductivity layer in the pasta region is not enough to delay the cooling. The difference is that in the accreting case the heating is over a long timescale so that the temperature of the inner crust is increased substantially. In the

magnetar case, the energy is deposited at the beginning of the outburst and the high temperature of the inner crust must be established rapidly.

We find that with our colder core temperature, the only way to get agreement with the ≈1000 day 2008 outburst measurement is to deposit energy directly into the inner crust during the 2008 outburst. The black curves in Figure 5 show models in which we extend the heating into the inner crust, depositing $E_{25} = 13$ in the inner crust but leaving the outer crust heating at $E_{25} = 1.0$ as before. Note that in this model the total energy deposited during the 2008 outburst is then comparable to the energy deposited in 1998, $\sim 10^{44}$ erg. The dramatic difference between the outburst light curves is due to the different radial distribution of the heating, rather than total energy. Although in the model shown we deposit energy throughout the inner crust, we find that we can match the observations as long as the crust is heated up to a density $\rho \lesssim 3 \times 10^{13}$ g cm^{-3}, so that the energetic requirements can be reduced by a factor of 2–3 compared to the model shown. These models predict that if the core temperature is low $T_{\rm core} \lesssim 7 \times 10^7$ K in SGR 1627-41, future observations should show a further decline in flux. We find that the future evolution is sensitive to the choice of $Q_{\rm imp}$ in the pasta layer and the choice of $T_c(\rho)$. This is shown by the black dashed, solid, and dotted–dashed curves in Figure 5 that have different choices for those parameters (these models are all consistent with the 1998 outburst, left panel of Figure 5).

4. Discussion

We have examined the late-time quiescent cooling of the neutron star transient MXB 1659-29 where cooling was observed for ≈4000 days into quiescence prior to its renewed outburst activity (Negoro et al. 2015). The quiescent cooling probes successively deeper layers of the neutron star's crust with increasingly longer thermal times and the late-time cooling ≳1000 days into quiescence depends on the thermal transport properties of the inner crust. In particular, late-time cooling in MXB 1659-29 requires a low thermal conductivity layer with $Q_{\rm imp} \gtrsim 20$ at mass densities $\rho \gtrsim 8 \times 10^{13}$ g cm^{-3} where nuclear pasta is expected to appear (Horowitz et al. 2015). The pasta layer maintains a temperature difference of $\Delta T \approx 3 \times 10^7$ K between the inner crust and core during the outburst. As a consequence, normal neutrons with a long thermal time appear at the base of the crust that cause late-time cooling if the neutron singlet pairing gap closes in the crust. Without normal neutrons at the base of the crust, as is the case if the neutron singlet pairing gap closes in the core, the crust reaches thermal equilibrium with the core after ≈3000 days and late-time cooling is removed.

Page & Reddy (2012) pointed out that differences in $T_c(\rho)$ and the resulting presence or absence of a layer of normal neutrons at the base of the crust could affect the cooling curves at late times ≈1000 days into cooling. We find a much larger effect and on a longer timescale here because the low thermal conductivity of the nuclear pasta layer keeps the inner crust much hotter during the outburst. During quiescence, the base of the crust remains at a higher temperature than the core for ≈5000 days (see Equation (5)). The temperature difference between the crust and core results in a slow decline of the quiescent light curve after ≳1000 days, as can be seen in Figure 1.

We also investigated the late-time cooling of KS 1731-260, which was observed ≈14.5 years into quiescence (Cackett et al. 2013). Although the quiescent light curve in this source can be fit without a low conductivity pasta layer (Merritt et al. 2016), we find a comparable fit with a $Q_{\rm imp} = 20$ pasta layer and using a neutron singlet pairing gap that closes in the crust (see Figure 4). That both MXB 1659-29 and KS 1731-260 fits prefer a pasta layer with $Q_{\rm imp} = 20$ suggests that the inner crust composition may be similar in accreting neutron stars regardless of their initial crust composition, as was found in a study of the accreted multi-component crust (Gupta et al. 2008).

We studied SGR 1627-41, a magnetar with late-time observations of two outbursts. Based on the previous outburst in 1998, the source may not yet have fully thermally relaxed and could show further cooling. We investigated a low conductivity pasta region as a way to prolong the cooling, but found that the flattening of the luminosity at times ≳1000 days could be explained only if energy was deposited directly into the inner crust. This is because in magnetars the energy is assumed to be deposited rapidly rather than over many thermal times as in accreting neutron stars. Nevertheless, if the core temperature is low, $T_{\rm core} \lesssim 7 \times 10^7$ K, variations in inner crust physics affect the light curve and should be included in models. Furthermore, the need for $\sim 10^{44}$ erg to be deposited in the inner crust constrains models for transient magnetic energy release in magnetars (e.g., Li et al. 2016; Thompson et al. 2016), and argues against only heating the crust externally (e.g., Li & Beloborodov 2015).

Late-time cooling in MXB 1659-29 requires that the $^1S_0$ neutron singlet pairing gap close in the crust. As a result, superfluid neutrons are confined to the inner crust shallower than the pasta layer at $\rho \lesssim 8 \times 10^{13}$ g cm^{-3} where $T \ll T_c$. By contrast, a recent study of pulsar glitches suggests that the neutron superfluid extends from the crust into the core continuously (Andersson et al. 2012). Recent calculations of the neutron effective mass in a non-accreted ($Q_{\rm imp} = 0$) crust suggest that $m_n^\star \gg m_n$ at the base of the crust (Chamel 2005, 2012). In this case, a larger fraction of free neutrons are entrained in the inner crust and the neutron superfluid must then extend into the core to supply adequate inertia for pulsar glitches (Andersson et al. 2012; Ho et al. 2015). We note, however, that the above calculation for the neutron effective mass is likely inappropriate for the impure crust compositions found in the accreting transients studied here. Therefore, we here assume $m_n^\star \approx m_n$ as found in Brown (2013) in the absence of effective mass calculations in an accreted crust.

The authors thank Hongjun An for useful comments on the manuscript. Support for A.D. and E.F.B. was provided by the National Aeronautics and Space Administration through *Chandra* Award Number TM5-16003X issued by the *Chandra X-ray Observatory* Center, which is operated by the Smithsonian Astrophysical Observatory for and on behalf of the National Aeronautics and Space Administration under contract NAS8-03060. A.D. and E.F.B. are also supported by the National Science Foundation under Grant No. AST-1516969. A.D. is also grateful for the support of the Michigan State University College of Natural Science Dissertation Completion Fellowship. A.C. is supported by an NSERC Discovery grant, is a member of the Centre de Recherche en Astrophysique du Québec (CRAQ), and an Associate of the CIFAR Cosmology and Gravity program. S.R. was supported by the U.S. Department of Energy under Contract No. DE-FG0200ER41132. This material is based upon work supported by the National Science Foundation under Grant

No. PHY-1430152 (JINA Center for the Evolution of the Elements).

Software: dStar (Brown 2015), MESA (Paxton et al. 2011, 2013, 2015), crustcool (https://github.com/andrewcumming/crustcool).

Appendix
Neutron Scattering Frequency in the Inner Crust

In this appendix, we derive expressions for the neutron scattering frequency in the inner crust. In the relaxation time approximation, the scattering frequency can be expressed as (Flowers & Itoh 1976; Potekhin et al. 1999)

$$\nu_n = \frac{m_n^\star}{12\pi^3\hbar^3}\frac{n_{\rm ion}}{n_n}\int_0^{2k_{{\rm F},n}} dq\, q^3\, |V(q)|^2\, S_\kappa(q), \tag{11}$$

where $\hbar q$ is the momentum transfer, $p_{{\rm F},n} = \hbar\,(3\pi^2 n_n)^{1/3} \equiv \hbar k_{{\rm F},n}$ is the neutron Fermi momentum, $m_n^\star$ is the effective neutron mass, n_n is the number density of neutrons outside of nuclei, $n_{\rm ion}$ is the number density of ions, and $V(q)$ is the the Fourier transform of the scattering potential. The scattering medium is described by the structure function

$$S_\kappa(q) = \int_{-\infty}^{\infty}\frac{d\omega}{2\pi}\frac{\hbar\omega}{k_{\rm B}T}\frac{S(q,\,\omega)}{1-\exp(-\hbar\omega/k_{\rm B}T)} \times\left[1+\left(\frac{\hbar\omega}{k_{\rm B}T}\right)^2\left(3\frac{k_{{\rm F},n}^2}{q^2}-\frac{1}{2}\right)\right], \tag{12}$$

which is written in terms of the dynamical structure factor $S(q,\,\omega)$.

To describe neutron–nucleus scattering in the inner crust, we assume that the nuclei are spherical and that the surface thickness is negligible compared to the size of the nucleus. Although the nuclei in the pasta phase are certainly non-spherical, a description of scattering in non-spherical geometries is beyond the scope of this paper. Under these assumptions, the potential seen by the neutrons can be modeled as a square well with $V(r<R_A) = V_0$, where R_A is the radius of the scattering center. The depth of the potential $V_0 \approx V_{\rm in} - V_{\rm out}$, where $V_{\rm in}$ and $V_{\rm out}$ are the neutron single particle potentials inside and outside the scattering structures, respectively. In the pasta phase, the density contrast between the scattering structure and the background rapidly decreases with increasing density, implying a correspondingly rapid decrease in V_0 and reduced neutron scattering.

With the spherical assumption, the effective neutron–nucleus potential in momentum space is

$$V_{n,A}(q) = V_0\frac{4\pi R_A^3}{3}F_A(qR_A), \tag{13}$$

with a form factor (Flowers & Itoh 1976)

$$F_A(x) = \frac{3[\sin(x) - x\cos(x)]}{x^3}. \tag{14}$$

The form factor $F_A \to 1$ in the limit that momentum transfers are small ($x = qR_A \ll 1$) and is suppressed when momentum transfers are large. Inserting Equation (13) into Equation (11), we find the neutron–phonon scattering frequency

$$\nu_{n,{\rm phn}} = \frac{4}{27\pi}\frac{m_n^\star c^2}{\hbar}\frac{n_{\rm ion}}{n_n}\left(\frac{V_0 R_A}{\hbar c}\right)^2\Lambda_{n,{\rm phn}}, \tag{15}$$

where the Coulomb logarithm is given by

$$\Lambda_{n,{\rm phn}} = \int_0^{2k_{{\rm F},n}R_A} dx\, x^3\, F_A^2(x)\, S_\kappa^{\rm phn}(q = x/R_A). \tag{16}$$

We evaluate the integral in Equation (16) using a Runge–Kutta scheme of order 8(5,3) (Hairer et al. 1993) and fitting formulae for $S_\kappa^{\rm phn}(q)$ (Potekhin et al. 1999, Equations (21) and (22)) that were developed in the context of electron–phonon scattering.

We find the frequency of neutron–impurity scattering using a similar approach. We assume that the impurities are uncorrelated elastic scatterers, and write the scattering frequency as a sum over all impurity species. The neutron–impurity potential for an impurity of species j with radius R_j is

$$V_{n,j} = V_0\frac{4\pi\bar{R}^3}{3}F_A(q\bar{R})\left(\frac{R_j^3}{\bar{R}^3}\frac{F_A(qR_j)}{F_A(q\bar{R})} - 1\right), \tag{17}$$

where $\bar{R}$ is the radius of the average ion in the lattice. With this assumption, the dynamical structure factor for impurity scattering is (Flowers & Itoh 1976)

$$S^{\rm imp}(q,\,\omega) = \frac{1}{n_{\rm ion}}\sum_j 2\pi n_j\delta(\omega), \tag{18}$$

where j is the sum over impurity species and n_j is the number density of impurities.

Upon using Equations (18) and (12) to obtain $S_\kappa^{\rm imp}(q) = \sum_j n_j/n_{\rm ion}$, and inserting $S_\kappa^{\rm imp}(q)$ and $V_{n,j}$ (Equation (17)) into Equation (11), we find the neutron–impurity scattering frequency

$$\nu_{nQ} = \frac{4}{27\pi}\frac{m_n^\star c^2}{\hbar}\frac{n_{\rm ion}}{n_n}\left(\frac{V_0\bar{R}}{\hbar c}\right)^2\Lambda_{nQ}\,\widetilde{Q}. \tag{19}$$

Here, we define the Coulomb logarithm for neutron–impurity scattering,

$$\Lambda_{nQ} = \int_0^{2k_{{\rm F},n}\bar{R}} dx\, x^3\, F_A^2(x), \tag{20}$$

and the impurity parameter for neutron scattering,

$$\widetilde{Q} = \frac{1}{\Lambda_{nQ}}\int_0^{2k_{{\rm F},n}\bar{R}} dx\, x^3\, F_A^2(x)\sum_j\frac{n_j}{n_{\rm ion}}\left(\frac{R_j^3}{\bar{R}^3}\frac{F_A(xR_j/\bar{R})}{F_A(x)} - 1\right)^2. \tag{21}$$

For scattering involving momentum transfers $q \lesssim 1/R_j$ the ratio $F_A(qR_j)/F_A(q\bar{R}) \approx 1$. Taking $R_j^3 \propto Z_j$ and $\bar{R}^3 \propto \langle Z\rangle$ then gives $\widetilde{Q} \approx Q_{\rm imp}/\langle Z\rangle^2$ where $Q_{\rm imp}$ (Equation (1)) is the impurity parameter for electron scattering. The neutron–impurity scattering frequency is therefore

$$\nu_{nQ} \approx \frac{4}{27\pi}\frac{m_n^\star c^2}{\hbar}\frac{n_{\rm ion}}{n_n}\left(\frac{V_0\bar{R}}{\hbar c}\right)^2\frac{Q_{\rm imp}}{\langle Z\rangle^2}\Lambda_{nQ}. \tag{22}$$

Since the neutron chemical potentials inside and outside the nucleus are required to be equal in Gibbs equilibrium, we can estimate V_0 as the difference in the single particle kinetic energies inside and outside the nucleus,

$$V_0 \approx \frac{\hbar^2(3\pi^2 n_{\rm in})^{2/3}}{2m_n}\left(1 - \left(\frac{n_n}{n_{\rm in}}\right)^{2/3}\right), \tag{23}$$

where $n_{\rm in}$ is the neutron number density inside the nucleus. We take R_A to be the proton radius of the nucleus given by $(4\pi/3)R_A^3 n_{\rm in} = Z$, where Z is the proton number of the nucleus. We therefore expect that $V_0 R_A/\hbar c \sim \mathcal{O}(1)$ in the inner crust. The total scattering frequency is

$$\begin{aligned}\nu_n = \nu_{n,\rm phn} + \nu_{nQ} &\approx \frac{4}{27\pi}\frac{m_n^\star c^2}{\hbar}\frac{n_{\rm ion}}{n_n}\left(\frac{V_0 R_A}{\hbar c}\right)^2 \\ &\times \left[\Lambda_{n,\rm phn} + \frac{Q_{\rm imp}}{\langle Z\rangle^2}\Lambda_{nQ}\right] \\ &= 6.7 \times 10^{20}\ {\rm s}^{-1}\left(\frac{m_n^\star}{m_n}\right)\left(\frac{n_{\rm ion}/n_n}{0.01}\right)\left(\frac{V_0 R_A}{\hbar c}\right)^2 \\ &\times \left[\Lambda_{n,\rm phn} + \frac{Q_{\rm imp}}{\langle Z\rangle^2}\Lambda_{nQ}\right]. \end{aligned} \quad (24)$$

The ratio of the phonon and impurity scattering frequencies is

$$\frac{\nu_{n,\rm phn}}{\nu_{nQ}} = \frac{\langle Z\rangle^2}{Q_{\rm imp}}\frac{\Lambda_{n,\rm phn}}{\Lambda_{nQ}} \quad (25)$$

and is typically of order unity for $Q_{\rm imp} \simeq 10$.

References

An, H., Kaspi, V. M., Tomsick, J. A., et al. 2012, ApJ, 757, 68
Andersson, N., Glampedakis, K., Ho, W. C. G., & Espinoza, C. M. 2012, PhRvL, 109, 241103
Baiko, D. A., Haensel, P., & Yakovlev, D. G. 2001, A&A, 374, 151
Baym, G., & Chin, S. A. 1976, NuPhA, 262, 527
Beloborodov, A. M. 2009, ApJ, 703, 1044
Bisnovatyĭ-Kogan, G. S., & Chechetkin, V. M. 1979, SvPhU, 22, 89
Brown, B. A. 2013, PhRvL, 111, 232502
Brown, E. F. 2015, dStar: Neutron Star Thermal Evolution Code, Astrophysics Source Code Library, ascl:1505.034
Brown, E. F., Bildsten, L., & Rutledge, R. E. 1998, ApJL, 504, L95
Brown, E. F., & Cumming, A. 2009, ApJ, 698, 1020
Cackett, E. M., Brown, E. F., Cumming, A., et al. 2013, ApJ, 774, 131
Cackett, E. M., Wijnands, R., Miller, J. M., Brown, E. F., & Degenaar, N. 2008, ApJL, 687, L87
Chamel, N. 2005, NuPhA, 747, 109
Chamel, N. 2012, PhRvC, 85, 035801
Chen, J. M. C., Clark, J. W., Davé, R. D., & Khodel, V. V. 1993, NuPhA, 555, 59
Cumming, A., Brown, E. F., Fattoyev, F. J., et al. 2017, PhRvC, 95, 025806
Flowers, E., & Itoh, N. 1976, ApJ, 206, 218
Gandolfi, S., Illarionov, A. Y., Fantoni, S., Pederiva, F., & Schmidt, K. E. 2008, PhRvL, 101, 132501
Gupta, S. S., Kawano, T., & Möller, P. 2008, PhRvL, 101, 231101
Gusakov, M. E., Yakovlev, D. G., Haensel, P., & Gnedin, O. Y. 2004, A&A, 421, 1143
Haensel, P., & Zdunik, J. L. 1990, A&A, 227, 431
Haensel, P., & Zdunik, J. L. 2003, A&A, 404, L33
Haensel, P., & Zdunik, J. L. 2008, A&A, 480, 459
Hairer, E., Norsett, S. P., & Wanner, G. 1993, Solving Ordinary Differential Equations I. Nonstiff Problems (2nd ed.; Berlin: Springer)
Hashimoto, M., Seki, H., & Yamada, M. 1984, PThPh, 71, 320
Ho, W. C. G., Espinoza, C. M., Antonopoulou, D., & Andersson, N. 2015, SciA, 1, e1500578
Horowitz, C. J., & Berry, D. K. 2008, PhRvC, 78, 035806
Horowitz, C. J., Berry, D. K., Briggs, C. M., et al. 2015, PhRvL, 114, 031102
Horowitz, C. J., Pérez-García, M. A., Carriere, J., Berry, D. K., & Piekarewicz, J. 2004, PhRvC, 70, 065806
Itoh, N., & Kohyama, Y. 1993, ApJ, 404, 268
Kouveliotou, C., Eichler, D., Woods, P. M., et al. 2003, ApJL, 596, L79
Leinson, L. B. 1993, ApJ, 415, 759
Li, X., & Beloborodov, A. M. 2015, ApJ, 815, 25
Li, X., Levin, Y., & Beloborodov, A. M. 2016, ApJ, 833, 189
Lyubarsky, Y., Eichler, D., & Thompson, C. 2002, ApJL, 580, L69
Maruyama, T., Niita, K., Oyamatsu, K., et al. 1998, PhRvC, 57, 655
Merritt, R., Cackett, E. M., Brown, E. F., et al. 2016, ApJ, 833, 186
Negoro, H., Furuya, K., Ueno, S., et al. 2015, ATel, 7943, 1
Newton, W. G., Murphy, K., Hooker, J., & Li, B.-A. 2013, ApJL, 779, L4
Ofengeim, D. D., Kaminker, A. D., & Yakovlev, D. G. 2014, EL, 108, 31002
Oyamatsu, K. 1993, NuPhA, 561, 431
Page, D., & Reddy, S. 2012, arXiv:1201.5602
Paxton, B., Bildsten, L., Dotter, A., et al. 2011, ApJS, 192, 3
Paxton, B., Cantiello, M., Arras, P., et al. 2013, ApJS, 208, 4
Paxton, B., Marchant, P., Schwab, J., et al. 2015, ApJS, 220, 15
Pons, J. A., & Rea, N. 2012, ApJL, 750, L6
Pons, J. A., Viganò, D., & Rea, N. 2013, NatPh, 9, 431
Potekhin, A. Y., Baiko, D. A., Haensel, P., & Yakovlev, D. G. 1999, A&A, 346, 345
Ravenhall, D. G., Pethick, C. J., & Wilson, J. R. 1983, PhRvL, 50, 2066
Rutledge, R. E., Bildsten, L., Brown, E. F., et al. 2002, ApJ, 580, 413
Sato, K. 1979, PThPh, 62, 957
Schneider, A. S., Horowitz, C. J., Hughto, J., & Berry, D. K. 2013, PhRvC, 88, 065807
Scholz, P., Kaspi, V. M., & Cumming, A. 2014, ApJ, 786, 62
Schwenk, A., Friman, B., & Brown, G. E. 2003, NuPhA, 713, 191
Thompson, C., Yang, H., & Ortiz, N. 2016, arXiv:1608.02633
Ushomirsky, G., & Rutledge, R. E. 2001, MNRAS, 325, 1157
Watanabe, G., Sato, K., Yasuoka, K., & Ebisuzaki, T. 2003, PhRvC, 68, 035806
Wijnands, R., Homan, J., Miller, J. M., & Lewin, W. H. G. 2004, ApJL, 606, L61
Wijnands, R., Nowak, M., Miller, J. M., et al. 2003, ApJ, 594, 952
Woods, P. M., Kouveliotou, C., van Paradijs, J., et al. 1999, ApJL, 519, L139